KAPL-P-000233
(K96137)

Hot-Film Anemometer Measurements in Adiabatic Two-Phase Flow through a Vertical Duct

CONF-970670--

T. A. Trabold, W. E. Moore, et. al.

June 1997

NOTICE

KAPL ATOMIC POWER LABORATORY SCHENECTADY, NEW YORK 12331

Operated for the U. S. Department of Energy
by KAPL, Inc. a Lockheed Martin company

DISCLAIMER

DISCLAIMER

Portions of this document may be illegible in electronic image products. Images are produced from the best available original document.

Hot-Film Anemometer Measurements in Adiabatic Two-Phase Flow through a Vertical Duct

Thomas A. Trabold, Wesley E. Moore and William O. Morris

Lockheed Martin Corporation
P.O. Box 1072
Schenectady, New York 12301

Abstract

A hot-film anemometer (HFA) probe was used to obtain local measurements of void fraction and bubble frequency in a vertically oriented, high aspect ratio duct containing R-134a under selected adiabatic two-phase flow conditions. Data were obtained along a narrow dimension scan over the range $0.03 \leq \overline{Z} \leq 0.80$, where $\overline{Z}$ is the distance from the wall normalized with the duct spacing dimension. The void fraction profiles displayed large gradients in the near-wall regions and broad maxima near the duct centerline. The trends in the bubble frequency data generally follow those for the local void fraction data. However, the relatively large number of bubbles at higher pressure implies a larger magnitude of the interfacial area concentration, for the same cross-sectional average void fraction. For the two annular flow conditions tested, analysis of the HFA output voltage signal enabled identification of three distinct regions of the flow field: liquid film with dispersed bubbles, interfacial waves, and continuous vapor with dispersed droplets.

Nomenclature

B	bias limit	w	mass flow rate
f_b	bubble frequency	X	streamwise dimension
P	test section static pressure	Y	transverse dimension
$S_{\overline{x}}$	precision index	Z	spacing dimension
t_{95}	student's t for 95% confidence	$\overline{Z}$	dimensionless distance from wall
T_{sat}	saturation temperature		
U	experimental uncertainty	α	local void fraction
V	HFA output voltage	$\overline{\alpha}$	cross-sectional average void fraction
V_T	threshold voltage		

1. Introduction

Gas-liquid two-phase flows are encountered in a variety of industrial applications, including chemical processing, petroleum transport and nuclear power generation. Computer codes are often used for process optimization and equipment design. However, successful application of these computer codes relies on the availability of an experimental database from which an understanding of fundamental physical phenomena can be developed. Such a database is also required to rigorously assess a code's predictive capability. Most of the experimental data presently available in the open literature apply to air-water flows through circular geometries at atmospheric conditions. For noncircular geometries, and for elevated temperature and pressure conditions, detailed two-phase flow data are seriously lacking.

Most of the measurement techniques available for local two-phase flow measurements have been designed for application in relatively large geometries under atmospheric test conditions. Improved techniques are required to extend these measurement capabilities to flow and geometric conditions that have not been extensively investigated in the past. Thermal anemometry instrumentation is well suited for local two-phase flow measurements, and its application in chlorinated (R-113 and R-114) and nonchlorinated (FC-72) refrigerant fluids has been reported previously (Dix, 1971; Shiralkar and Lahey, 1972; Hasan *et al.*, 1991; de Carvalho and Bergles, 1992; Trabold *et al.*, 1994). The hot-film anemometer is one of the primary instruments in Lockheed Martin Corporation's R-134a (SUVA[1]) test facility.

This paper documents experiments which were performed in a vertical, high aspect ratio duct under adiabatic flow conditions. The duct had a hydraulic diameter of 0.485 cm and an aspect ratio of 22.5. Heat was applied upstream of the test section to create a two-phase flow of known cross-sectional average void fraction. These adiabatic tests provided a relatively simple platform for initial operation of advanced instrumentation, and represented a convenient baseline for more extensive testing under specific adiabatic and wall-heated flow configurations. Although a variety of measurement techniques, including gamma densitometry, laser Doppler velocimetry and high-speed video, was employed in this test facility, the focus of the present work was to develop hot-film anemometry methods for measurements of various thermal-hydraulic parameters over a wide range of flow conditions. The data thus obtained are useful for development of physical models for multi-field two-phase flow computer codes.

2. Description of Measurement Technique

A constant temperature anemometry (CTA) system typically consists of a probe which is directly exposed to the two-phase flow field, electronic circuitry which controls the amount of heating current supplied to the probe, an analog-to-digital converter and a PC-based data acquisition system. The sensitive element of a thermal anemometry probe is a thin sensor which is suspended across two needles. Gold plating near the supports serves the dual functions of strengthening the sensor and concentrating the resistance at the center of the sensor where local measurements are made. When fluid passes the probe, this sensor is cooled, resulting in a decrease in its resistance. An

1. SUVA® is a trademark of Dupont Chemicals for 1,1,1,2-tetrafluoroethane.

amplifier in the resistive bridge circuit instantaneously increases the current through the sensor to maintain it at a constant temperature. Since the cooling capacities of the vapor and liquid in a two-phase mixture are quite different, a distinct change in the voltage signal is observed depending on which phase envelopes the sensor at any instant in time. A typical output voltage trace is shown in Figure 1, where the upper and lower voltage levels correspond to the liquid and vapor phases, respectively. An analog-to-digital converter produces a digital record of the voltage signal which can be analyzed to provide a measurement of the local void fraction and bubble frequency, as described below.

The initial attempts at using thermal anemometry in the present test program involved both tungsten and platinum-iridium hot-wire sensors. Although measurements had previously been made in R-114 flows (Trabold *et al.*, 1994), these sensors proved to be too fragile to operate over extended periods for these experiments, due to the significantly higher fluid velocities. It was therefore decided to employ more sturdy quartz fiber hot-film probes which were subsequently found to survive longer, without appreciably affecting signal quality.

Hot-film anemometer (HFA) void fraction data were obtained using a single probe in spacing (Z dimension) scans at the center of the duct width, near the test section exit (Figure 2). The effective hydrodynamic entrance length at this position is $246D_H$. The HFA probe employed during these tests consisted of a single quartz fiber platinum-coated sensor with diameter of 25.4 μm and active length of 254 μm. A pin bent 90° downstream on the HFA probe provided a means of positioning the sensor by sensing contact with a transparent, electrically conducting film attached to the opposing window. For the experiments documented here, the probe was traversed over the spacing range of $0.03 \leq \overline{Z} \leq 0.80$, where $\overline{Z}$ is the distance from the wall normalized by the duct spacing dimension. Movement was limited to $\overline{Z} \leq 0.80$ to preclude contact between the curved part of the needles supporting the sensor and the edge of the hole in the quartz window.

A number of techniques for analysis of the thermal anemometer signal in two-phase flow have been proposed. The proper analysis technique depends on the characteristics of the HFA output voltage signal. For previous measurements in R-114, level thresholding was used since the fall and rise times in the output signal were so short (generally in the range 30 to 70 μs) that a nearly square-wave response was observed. A threshold voltage (V_T) was established such that for $V > V_T$, the active element of the HFA probe was considered to be in contact with liquid. Conversely, for $V \leq V_T$, the probe was in contact with the vapor phase. The number of discrete voltages for which $V \leq V_T$ divided by the total number of samples in a given measurement period represented the residence time fraction of the vapor phase, which was directly analogous to the local void fraction (Jones and Zuber, 1978).

Even though significantly higher interfacial velocities were encountered in the present test than those previously made in R-114, the voltage waveforms associated with the present measurements showed rise and fall times due to bubble-probe interaction which were about an order of magnitude longer. The general form of the HFA voltage signal can be explained by reference to the mechanics of a bubble interacting with the active probe element, as shown in Figure 1. For the hot-film to penetrate either the front or rear vapor-liquid interface, surface tension must be overcome. After penetrating the front interface, the thin liquid layer remaining on the sensor is boiled off. These two phenomena are controlled by the liquid surface tension and heat of vaporization, respectively. Even though the surface tension of R-134a is lower than that of R-114 (8.2 and 12

dyne/cm at 25°C, respectively), the heat of vaporization at the boiling point is higher (217 and 136 kJ/kg, respectively). Since these two physical property effects tend to counteract each other, the longer rise and fall times observed in this investigation are believed to be primarily due to the presence of smaller bubbles which make the liquid-vapor interfaces more difficult to penetrate.

In order to account for longer rise and fall times in the current work, the signal analysis method of de Carvalho and Bergles (1992) was used, in which phase changes were identified by level thresholding, and slope thresholding was used to account for the void volume passage time. For experiments conducted in pool boiling of FC-72, these authors analyzed the signals by first setting a threshold voltage (V_T) whereby for $V \leq V_T$ the probe was considered to be in contact with vapor. Additionally, they proposed including voltage samples on either side of the negative bubble pulses until the slope changed sign. Once the raw voltage signal was converted into the phase indicator function (i.e., I = 0 for liquid, -1 for vapor), the number of voltage samples for which the vapor phase was present at the probe divided by the total number of voltage samples gave a measurement of the local ensemble-averaged vapor volume fraction. Addtionally, the number of negative pulses in the phase indicator function per unit time provides a measurement of the bubble frequency, which enters into calculation of the mean bubble size and interfacial area concentration.

The most important part of the analysis procedure for void fraction calculation is the proper selection of the threshold voltage, V_T. For a given set of flow and pressure conditions, V_T may be determined by plotting the voltage sample histogram, a typical example of which is shown in Figure 3. The most probable vapor and liquid voltages are represented by the left and right peaks, respectively. As recommended by Trabold *et al.* (1994), V_T is selected as the voltage at the midpoint between these two peaks. For the present measurements, the computed void fraction was generally independent of V_T in the range of voltages between the peaks in the voltage sample histogram.

The nominal test conditions for the present adiabatic flow experiments are summarized in Table 1. In each case, the loop heaters immediately upstream of the test section were used to create a two-phase mixture of known inlet average void fraction. During the course of HFA measurements, a gamma densitometer system (GDS) was employed to obtain measurements of cross-sectional average void fraction at four elevations: X = 21.2, 51.7, 82.1 and 112.6 cm. This instrument relates the attenuation of a gamma beam to the density of the two-phase mixture ($\rho_{2\phi}$), from which the void fraction averaged along the direction of beam propagation is calculated by the expression

$$\bar{\alpha} = \frac{\rho_l - \rho_{2\phi}}{\rho_l - \rho_g} \tag{1}$$

where ρ_l and ρ_g are, respectively, densities of the pure liquid and vapor phases. Also, for selected test runs, a line-average GDS measurement was made at the center of the duct width at X =112.6 cm, immediately beneath the HFA probe. This provided a means of directly comparing the line-average void fractions obtained by these two instruments.

3. Results and Discussion

Local void fraction and bubble frequency data were obtained under adiabatic (i.e., no wall heat input) conditions with the nominal mass flow rates, pressures and inlet void fractions given in Table 1. The data are presented for each mass flow rate and pressure combination in Figures 4 through 7. All data are plotted as a function of the dimensionless distance from the wall, that is the Z position normalized with the duct spacing dimension ($\overline{Z}$). Since the tendency toward phase separation in high void fraction flows made the bubble frequency difficult to interpret, f_b data are reported only for nominal inlet void fractions of 0.1, 0.3 and 0.5. Additional information on the actual test conditions is provided in the table shown in part (a) of each figure. The nominal inlet void fraction and void fraction at X = 112.6 cm shown in the table are cross-sectional average values, the latter being measured with the gamma densitometer system. A plot of the streamwise development of the cross-sectional average void fraction measured with the GDS is also shown in part (b) of the figures. For some cases, an accurate measurement of the quality was not obtainable.

Attention is first directed to the trends in the cross-sectional average void fraction data, obtained with the gamma densitometer, illustrated in Figures 4(b) through 7(b). For most test conditions, particularly for low inlet qualities, the cross-sectional average void decreased as a function of streamwise position (X) due to heat transfer between the test fluid and the ambient environment. For example, at a pressure of about 1.35 MPa ($T_{sat} \approx 52\ ^{o}C$), a decrease in $\overline{\alpha}$ by as much as half or more was measured for inlet void fractions of 0.1 and 0.3, due to heat loss (Figure 4b). Also, for the case of P = 2.35 MPa ($T_{sat} \approx 75\ ^{o}C$), significant streamwise reductions in $\overline{\alpha}$ were also observed for void fractions of 0.3 and 0.5 (Figure 7b).

With the exception of the 0.1 inlet void case at P = 1.35 MPa and w = 53 kg/hr (Figure 4), the local HFA void fraction and bubble frequency profiles were all characterized by large gradients in the near-wall region ($\overline{Z} < 0.20$), and flatter profiles in the neighborhood of the duct centerline. Differences in the local void fraction profiles for the same inlet void fraction were due to significant variations in the flow structure in the Y dimension (e.g., large slugs in the center of the duct with nearly all-liquid regions near the edges), and condensation due to test section heat losses. As mentioned above, the condensation effect was most pronounced for inlet void fractions of 0.1, 0.3 and 0.5. For these cases, significant differences in the α profiles were observed. Unlike the lower average void fraction runs, the profiles for $\overline{\alpha}$ = 0.7 and 0.9 were much less affected by condensation.

Most of the results for moderate inlet void fractions (0.3, 0.5 and 0.7) showed a sinusoidal variation of the local void fraction across the Z dimension. This is due to the fact that the vapor volumes which interact with the probe occupied the entire duct thickness. A notable exception is for the case of w = 106 kg/hr, P = 2.35 MPa and $\overline{\alpha}$ = 0.3 (Figure 7c) where the relatively low local void fractions measured suggest that the HFA probe is exposed to a dispersed bubbly flow field with vapor volumes that are smaller than the duct thickness.

The trends in the bubble frequency data generally followed those associated with the local void fraction data. Two exceptions are worthy of note. First, for a nominal inlet void fraction of 0.3, the bubble frequency data for P = 2.35 MPa and w = 106 kg/hr (Run 70, Figure 7d) agreed with the results for the other three pressure/flow combinations within ± 20 Hz, even though the associated void fraction profile (Figure 7c) lies well below the $\overline{\alpha}$ = 0.3 data in Figures 4(c), 5(c) and 6(c).

Second, for the same pressure and flow conditions with $\overline{\alpha} = 0.5$, the bubble frequency was nearly 100% greater at the duct centerline than for the other flow and pressures tested. That this is true, even though the void fraction profiles were in much closer agreement, indicates that the flow field for P = 2.35 MPa and w = 106 kg/hr was comprised of a much greater number of smaller bubbles for roughly the same vapor volume fraction. The relatively large number of bubbles at high pressure implies a larger magnitude for the interfacial area concentration, for the same $\overline{\alpha}$.

For the adiabatic tests documented in this report, two were run with a nominal inlet void fraction of 0.9 (Run 61, Figure 6; Run 69, Figure 7). Both profiles were characterized by large void fraction gradients near the wall, and a nearly constant void fraction close to unity over the center half of the duct. This is indicative of a phase separation between mainly continuous liquid flowing along the walls, and a primarily continuous vapor region centered about the duct axis. Since Runs 61 and 69 in Figures 6 and 7, respectively, were obtained at different system pressures, the difference in void profiles between Runs 61 and 69 over the region $0.05 < \overline{Z} < 0.20$ suggests that there were also differences in the mean liquid film thickness and interfacial wave behavior which were dependent on system pressure.

Aside from the detailed local void fraction data obtained in the near-wall region, it was also possible to extract additional information from further analysis of the HFA output signal. For example, oscilloscope traces could be used to construct a conceptual picture of the various parts of the annular flow field, a sketch of which is given in Figure 8. At $\overline{Z} = 0.03$, the HFA output voltage waveform indicated a primarily liquid region (characterized by a relatively high voltage) in which negative voltage pulses occurred due to the presence of dispersed bubbles. At $\overline{Z} = 0.10$, the majority of the output signal was comprised of relatively low voltage samples, indicative of the vapor phase, with large peaks which were associated with the passage of interfacial waves. At $\overline{Z} = 0.50$, the waveform showed a fairly steady low level (vapor) voltage upon which was superimposed periodic positive pulses indicative of the dispersed droplet field.

Additional insight into the structure of the annular flow field could be gained by the change in the output voltage sample histograms as a function of distance from the wall, as illustrated in Figure 9. At $\overline{Z} = 0.03$, the voltage histogram was indicative of a bubbly flow field, with a peak at a relatively high voltage and a smaller broad peak in the lower voltage range. At $\overline{Z} = 0.10$, a large narrow peak developed at a low voltage, indicative of the vapor phase. It is believed that this arose from the contact of the HFA sensor with the bottom of the troughs in the interfacial waves. This supposition was supported by the change in the voltage histogram as the probe was moved further away from the wall; the narrow, low voltage peak became more dominant as the broad liquid peak was continually diminished. This was the expected behavior as the probe was moved through the region of interfacial waves away from the continuous liquid field. At $\overline{Z} = 0.50$, the histogram was characterized by a single narrow peak associated with a rather steady vapor voltage level. The voltage samples to the right of this peak corresponded to the voltage spikes resulting from the interaction of the HFA sensor with dispersed liquid droplets.

Frequency analysis of the raw HFA voltage signal provided additional insight into the characteristics of the interfacial wave field, which can be expected to affect the interphase and interfield transfer mechanisms, and contribute significantly to the interfacial area concentration. A double sensor HFA probe afforded measurement of mean interfacial velocity by the most probable time

shift between the two output signals, as ascertained from the cross-correlation spectrum. Such an approach in annular flow should provide data on wave propagation velocity. Similarly, the dominant peak in the autocorrelation spectrum (obtained using the upstream sensor only) will give the mean wave frequency. This measurement was made for a single annular flow test run (Figure 10). The approximately 30 Hz frequency thus obtained was confirmed by high speed video records of the passing waves. Combined with the visual wave spacing, an estimate of the wave velocity may be obtained.

Due to the central importance of the hot-film anemometer technique in the current experimental program, it was necessary to quantify the measurement uncertainty associated with this device. The measurement uncertainty may be calculated using the root-sum-square uncertainty interval:

$$U = \pm[B^2 + (t_{95}S_{\bar{x}})^2]^{1/2} \tag{2}$$

The precision limit ($t_{95}S_{\bar{x}}$) can be derived from the standard deviations of repeat measurements. According to Dieck (1992), when there are m redundant measurements with varying numbers of repeats, the overall ("pooled") standard deviation can be calculated by

$$S_{pooled} = \left(\frac{\nu_1 S_1^2 + \nu_2 S_2^2 + \ldots + \nu_m S_m^2}{\nu_1 + \nu_2 + \ldots + \nu_m} \right)^{1/2} \tag{3}$$

where S_1, S_2, ..., S_m are the individual standard deviations and ν_1, ν_2, ..., ν_m the associated degrees of freedom. The degrees of freedom for each standard deviation (υ) equal n -1, where n is the number of samples used to calculate each individual standard deviation.

To calculate the pooled standard deviation, use was made of the few repeat measurements obtained in the present adiabatic flow experiments as well as more recent tests where larger samples of repeat measurements were acquired. From these data, S_{pooled} for void fraction was calculated to be 0.96% in void fraction. The precision index is then computed by

$$S_{\bar{x}} = \frac{S_{pooled}}{\sqrt{N}} \tag{4}$$

where N is the number of samples (i.e., individual standard deviations calculated), leading to $S_{\bar{x}} = 0.43\%$ in void fraction. The degrees of freedom associated with the precision index is $\upsilon_{pooled} = \Sigma\upsilon_i = 37$ and therefore, $t_{95} = 2.0$. The precision limit ($P = t_{95}S_{\bar{x}}$) for void fraction measurements is then equal to 0.0086. A similar approach was used to determine the precision of bubble frequency measurements, yielding $P = 6.1$ Hz.

The bias limits (B) for hot-wire anemometry measurements are more difficult to quantify since we are forced to rely on error estimation. In the case of void fraction, the bias error due to the method of threshold voltage determination is expected to be no more than 0.02 since the variation of the calculated void fraction with V_T was demonstrated to be small (Figure 3). Other sources of bias error and their estimated contributions to void fraction error are: deflected bubbles which are not

penetrated by the hot-film sensor (0.01) and too short a time trace to capture low frequency void fraction fluctuations, which could also be affected by a bias in the measured test section mass flux (0.01). Using the root-sum-square method, the estimated bias limit is therefore 0.024, leading to an uncertainty (Equation 2) for void fraction of $U_\alpha = \pm 0.025$. An additional bias error is associated with the bubble frequency (f_b) measurement. Very small bubbles which do not envelop the entire HFA sensor may produce negative voltage pulses which are not accounted for by the level threshold used in the signal analysis program. Although these small bubbles may have little effect on the void fraction measurement, they could result in a significant error in f_b. Since this component of the bias would only result in a negative error, the bias limit is unsymmetrical, and estimated to be -10 Hz to +5 Hz. These values lead to an uncertainty band based on the root-sum-square model of U_{fb} = - 11.7 to +7.9 Hz.

Additional insight into the uncertainty associated with the HFA void fraction measurements can be obtained by comparing the integrated average data to the line-average void fraction from the gamma densitometer. Such a comparison is shown in Figure 11, where the line-average HFA data were determined by numerical integration using the trapezoid rule. The average difference between the two sets of void fraction data is 0.03, with all but the lowest HFA measurement falling within the established GDS uncertainty band. In bubbly flow, the somewhat higher HFA void fraction data may be due to inaccuracy in the determination of void passage time. The smaller bubbles may be impeded slightly during bubble-probe interaction, which would increase the apparent void passage time and hence, local void fraction.

4. Conclusions

It has been established that the hot-film anemometry technique is capable of acquiring important thermal-hydraulic data in two-phase refrigerant fluid flows, in bubbly, transitional and annular flow regimes. Local void fraction and bubble frequency data were obtained for four different pressure/flow test conditions. The void fraction data generally displayed large gradients in the near-wall regions with fairly flat profiles in the vicinity of the duct center plane. The bubble frequency profiles were largely similar to those measured for void fraction. However, there was evidence of a greater number of bubbles at the highest pressure condition, which would suggest a greater magnitude of the local interfacial area concentration for a roughly equivalent vapor velocity. Further analysis of the HFA output voltage signals and voltage sample histograms in annular flow demonstrated the existence of three distinct flow field structures: continuous liquid film with dispersed bubbles, interfacial waves and continuous vapor core with dispersed liquid droplets. The experimental results reported in this paper have provided a convenient baseline for more complex testing conducted to construct a fundamental thermal-hydraulic database for two-fluid model computer codes.

Acknowledgment

The authors acknowledge the valuable contributions of Messrs. L. Jandzio, E. Hurd and C.W. Zarnofsky in the operation of the test facility and acquisition of hot-film anemometer and gamma densitometer system data.

References

de Carvalho, R. and Bergles, A.E., "The Pool Nucleate Boiling and Critical Heat Flux of Vertically Oriented, Small Heaters Boiling on One Side," Rennselaer Polytechnic Institute, Heat Transfer Laboratory Report HTL-12, August 1992.

Dieck, R.H., *Measurement Uncertainty - Methods and Applications*, Instrument Society of America, Research Triangle Park, NC (1992).

Dix, G.E., "Vapor Void Fractions for Forced Convection with Subcooled Boiling at Low Flow Rates," Ph.D. Thesis, University of California, Berkeley (1971).

Hasan, A., Roy, R.P. and Kalra, S.P., "Some Measurements in Subcooled Flow Boiling of Refrigerant-113," *J. Heat Trans.*, Vol. 113, pp. 216-223 (1991).

Jones, O.C. and Zuber, N., "Use of a Cylindrical Hot-Film Anemometer for Measurement of Two-Phase Void and Volume Flux Profiles in a Narrow Rectangular Channel," *Heat Transfer: Research and Application,* AIChE Symposium Series, Vol. 74, No. 174, pp. 191-204 (1978).

Shiralkar, B.S. and Lahey, R.T., Jr., "Diabatic Local Void Fraction Measurements in Freon-114 with a Hot-Wire Anemometer," *ANS Trans.*, Vol. 15, p. 880 (1972).

Trabold, T.A., Moore, W.E., Morris, W.O., Symolon, P.D., Vassallo, P.F. and Kirouac, G.J., "Two Phase Flow of Freon in a Vertical Rectangular Duct. Part II: Local Void Fraction and Bubble Size Measurements," *Experimental and Computational Aspects of Validation of Multiphase Flow CFD Codes*, I. Celic *et al.* (Editors), FED-Vol. 180, pp. 67-76, ASME (1994).

Table 1 - Nominal Conditions for HFA Measurements

Run No.	Mass Flow (kg/hr)	Pressure (MPa)	Inlet Void Fraction (%)
63	53	1.35	10
62	53	1.35	30
65	53	1.35	50
66	53	1.35	70
72	106	0.59	30
73	106	0.59	50
58	106	1.35	10
59	106	1.35	30

Run No.	Mass Flow (kg/hr)	Pressure (MPa)	Inlet Void Fraction (%)
57	106	1.35	50
60	106	1.35	70
61	106	1.35	90
70	106	2.35	30
67	106	2.35	50
68	106	2.35	70
69	106	2.35	90

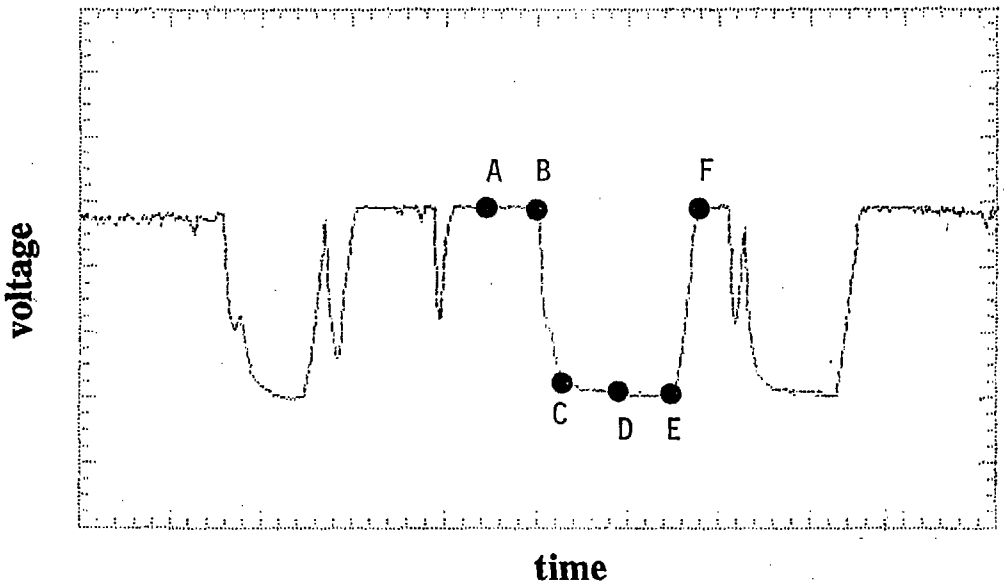

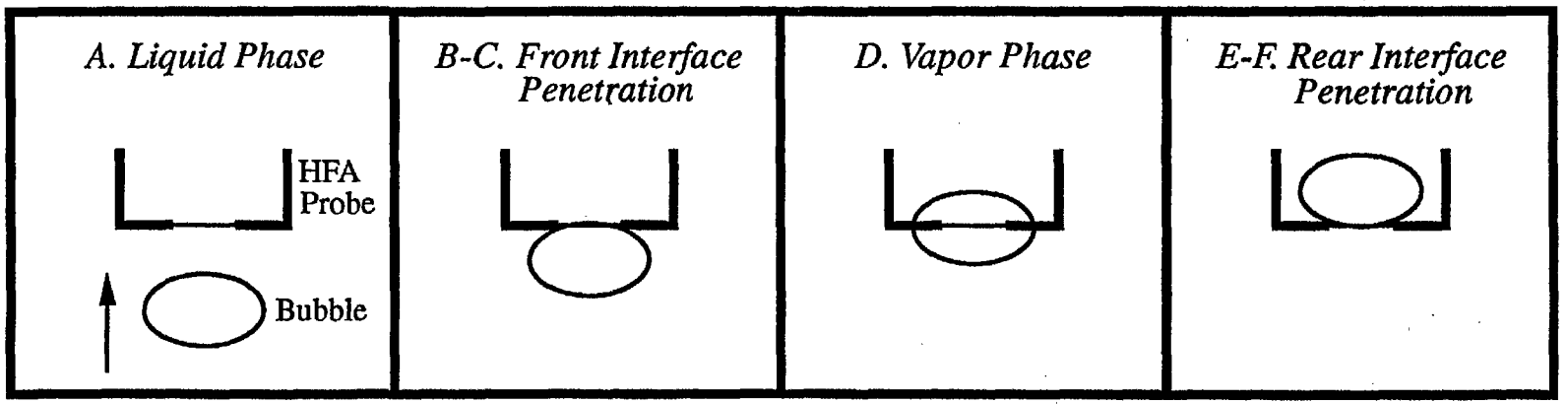

Figure 1 - Hot-Film Anemometer Output Signal and Bubble-Probe Interaction

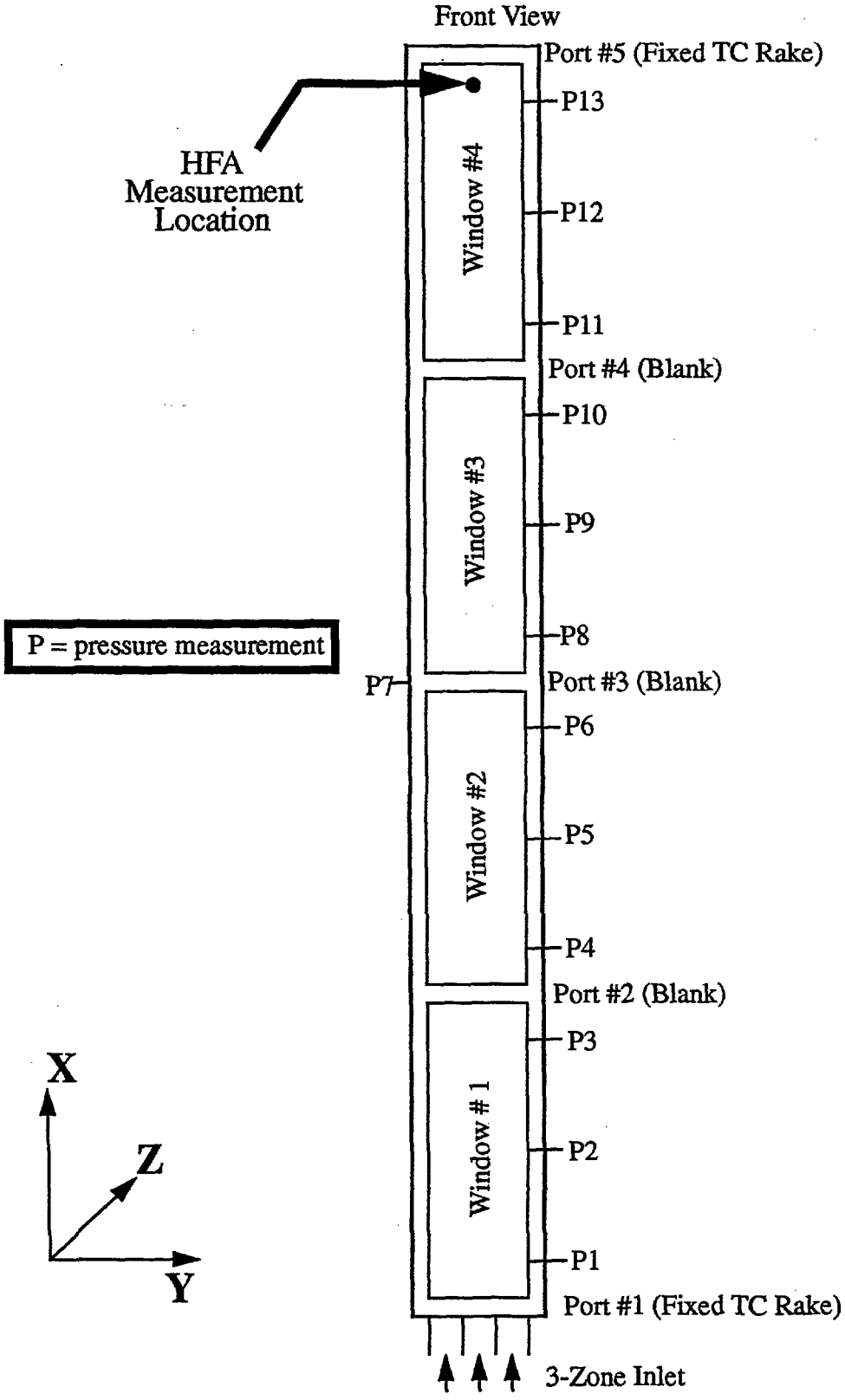

Figure 2 - Test Section and Measurement Locations

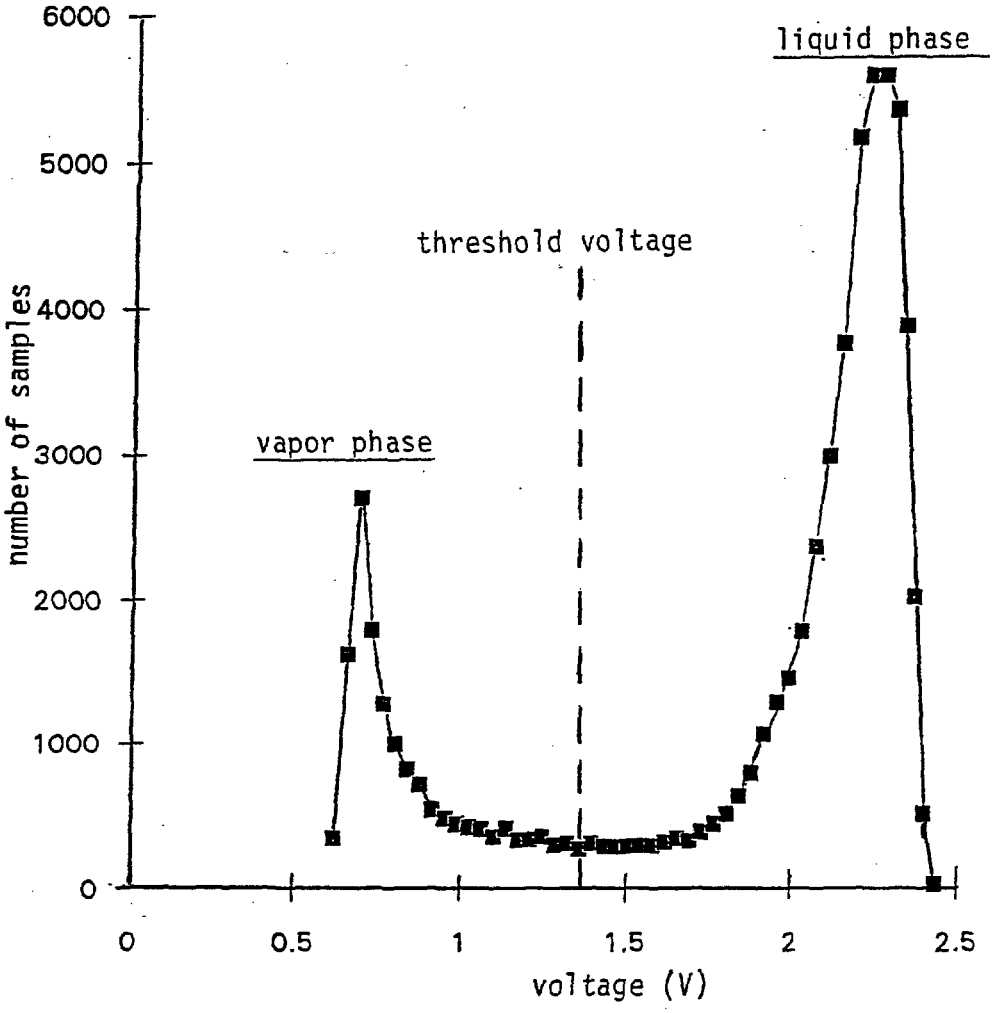

Figure 3 - Typical Voltage Sample Histogram
(Run 58, $\overline{Z} = 0.50$)

Run	Mass Flow Rate (kg/hr)	Exit Pressure (MPa)	Inlet $\bar{\alpha}$ (nominal)	$\bar{\alpha}$ at $X = 112.6$ cm	Inlet Quality	Exit Quality
63	53.5	1.35	0.1	0.029		
62	53.2	1.35	0.3	0.100	0.178	0.044
65	53.3	1.35	0.5	0.411	0.282	0.155
66	54.2	1.34	0.7	0.685	0.439	0.333

(a)

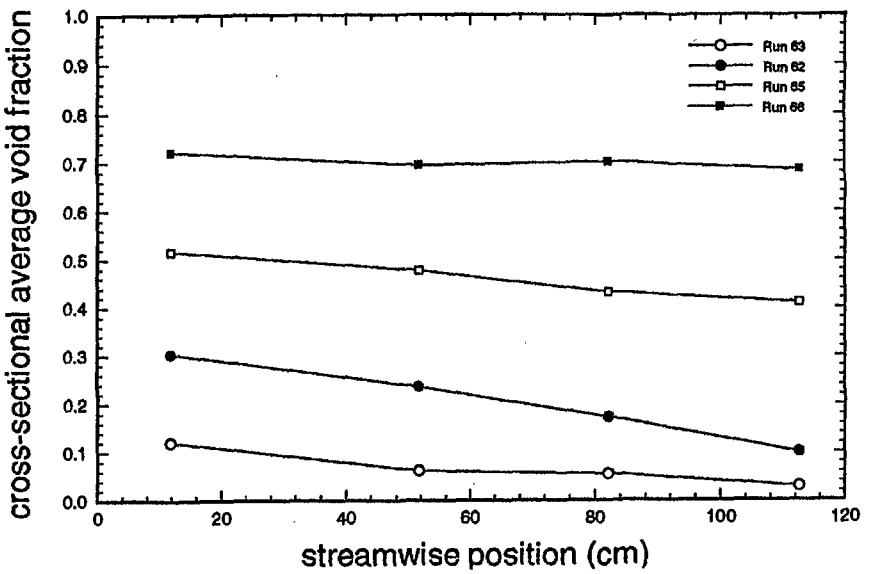

(b)

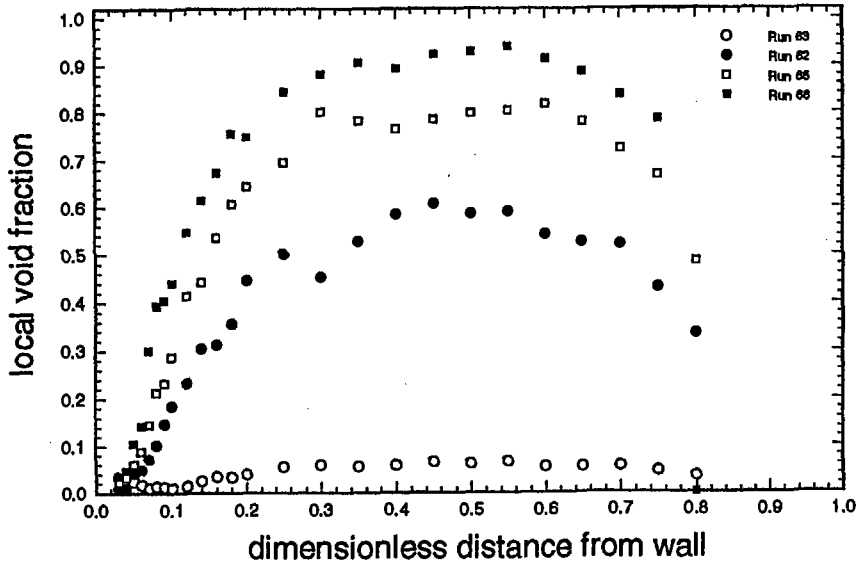

(c)

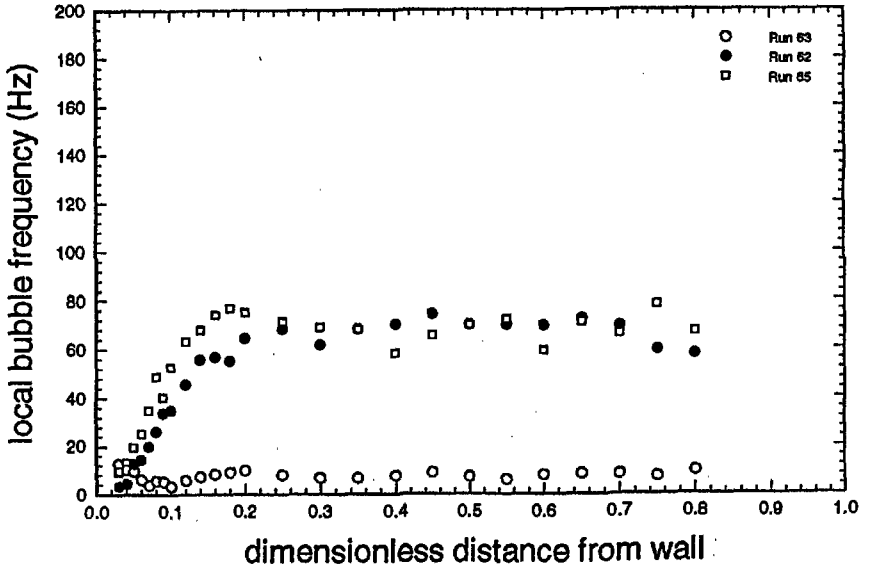

(d)

Figure 4

Run	Mass Flow Rate (kg/hr)	Exit Pressure (MPa)	Inlet $\bar{\alpha}$ (nominal)	$\bar{\alpha}$ at $X = 112.6$ cm	Inlet Quality	Exit Quality
72	105.7	0.58	0.3	0.343		
73	106.5	0.59	0.5	0.530	0.047	0.062

(a)

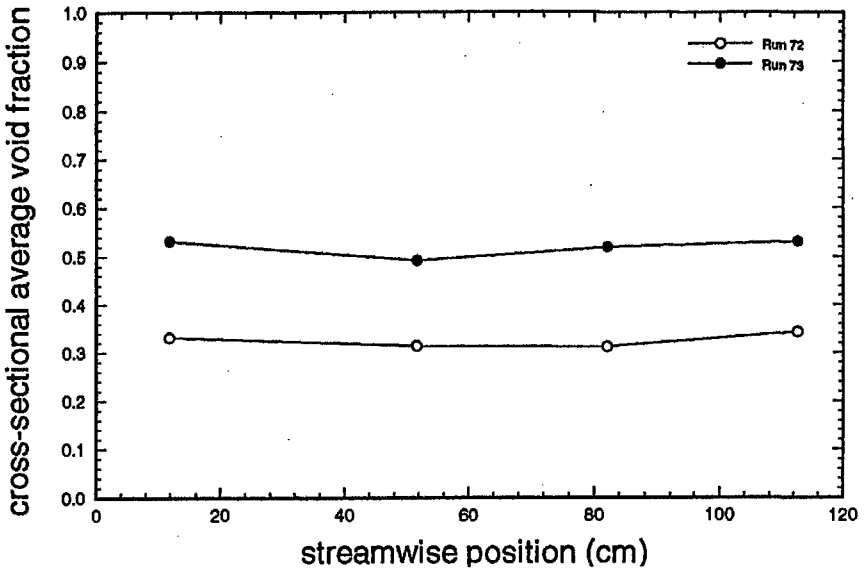

(b)

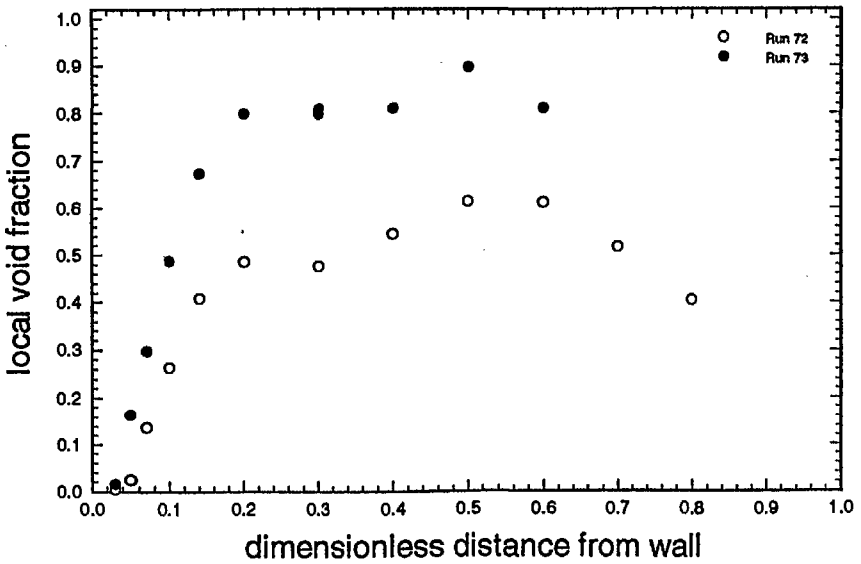

(c)

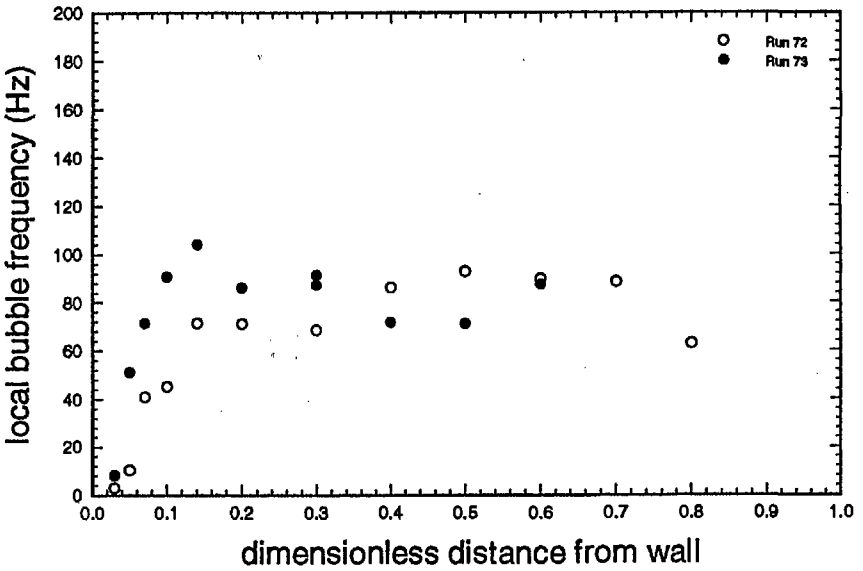

(d)

Figure 5

Run	Mass Flow Rate (kg/hr)	Exit Pressure (MPa)	Inlet $\bar{\alpha}$ (nominal)	$\bar{\alpha}$ at $X = 112.6$ cm	Inlet Quality	Exit Quality
58	103.9	1.36	0.1	0.016		
59	105.5	1.34	0.3	0.213	0.107	0.038
57	106.1	1.34	0.5	0.458	0.185	0.109
60	105.3	1.35	0.7	0.631	0.310	0.237
61	106.0	1.35	0.9	0.915	0.681	0.613

(a)

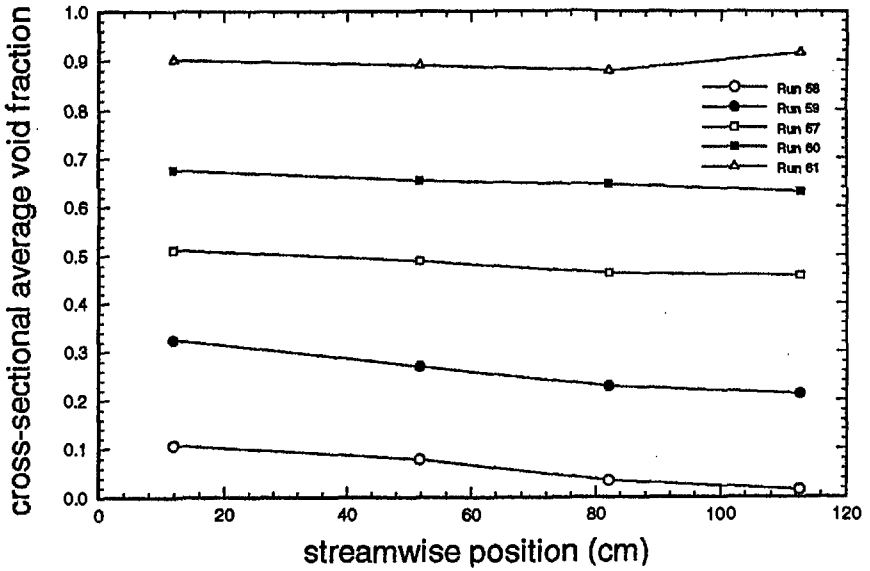

(b)

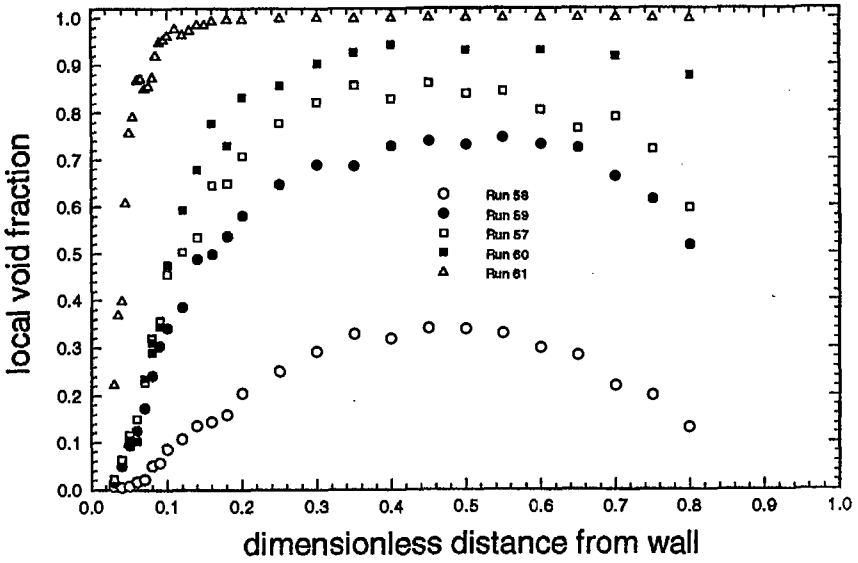

(c)

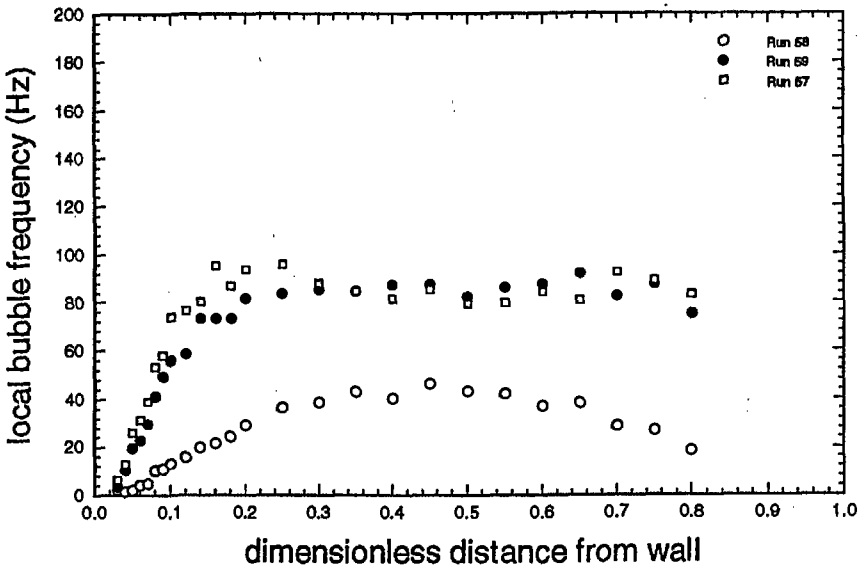

(d)

Figure 6

Run	Mass Flow (kg/hr)	Exit Pressure (MPa)	Inlet $\bar{\alpha}$ (nominal)	$\bar{\alpha}$ at $X = 112.6$ cm	Inlet Quality	Exit Quality
70	106.7	2.35	0.3	0.052		
67	106.6	2.35	0.5	0.347	0.268	0.101
68	106.7	2.36	0.7	0.641	0.426	0.264
69	106.0	2.34	0.9	0.907	0.926	0.765

(a)

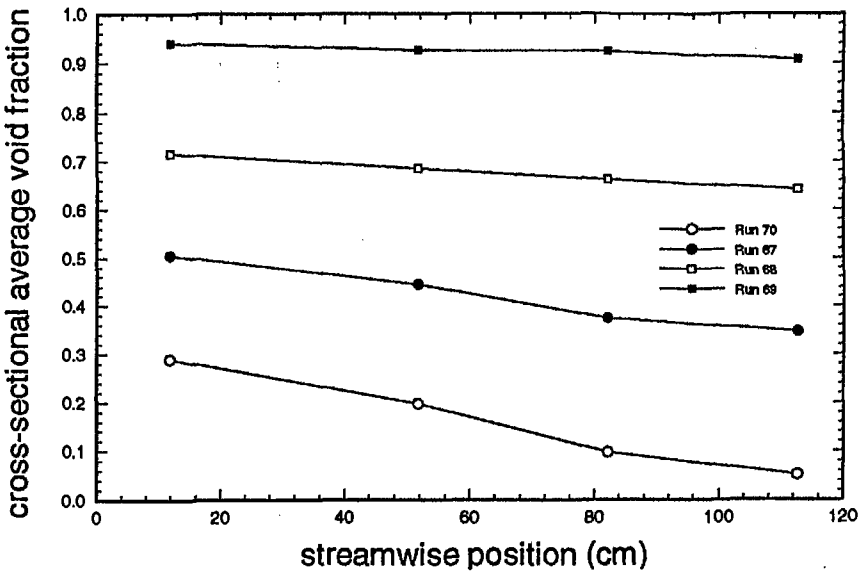

(b)

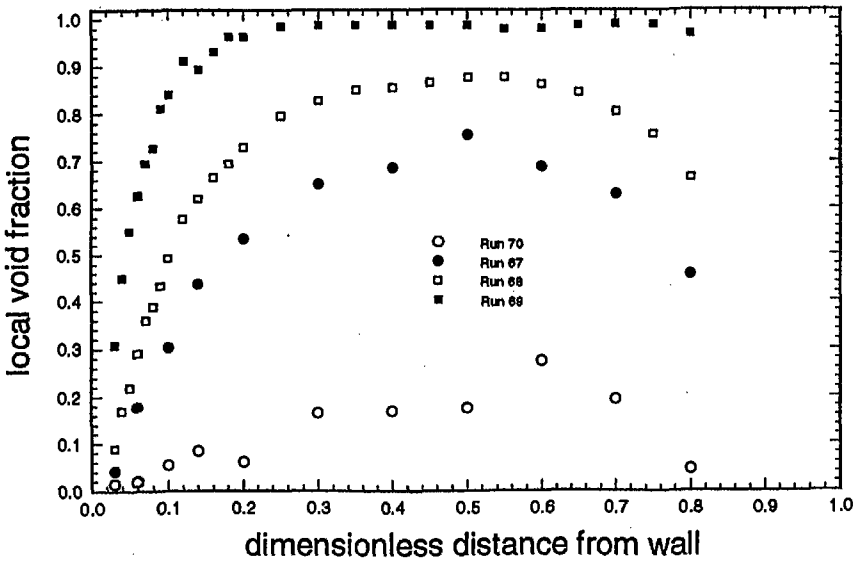

(c)

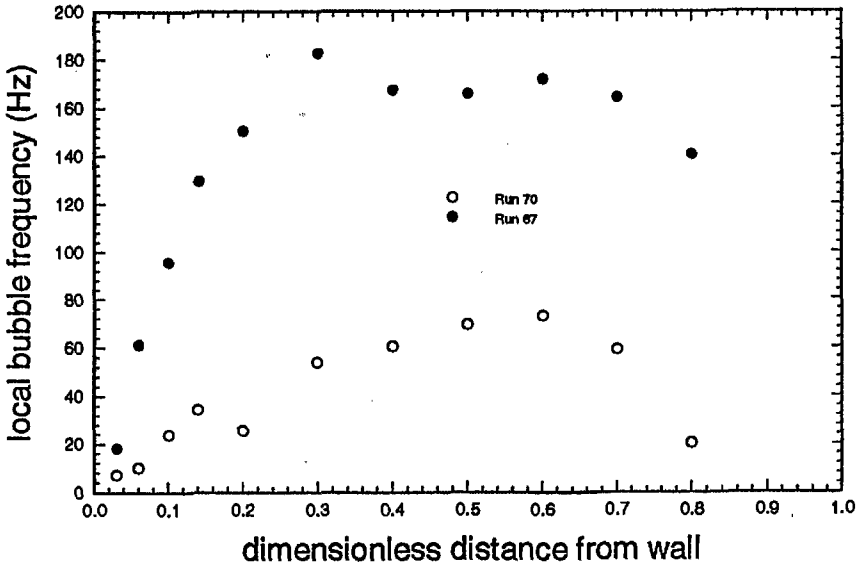

(d)

Figure 7

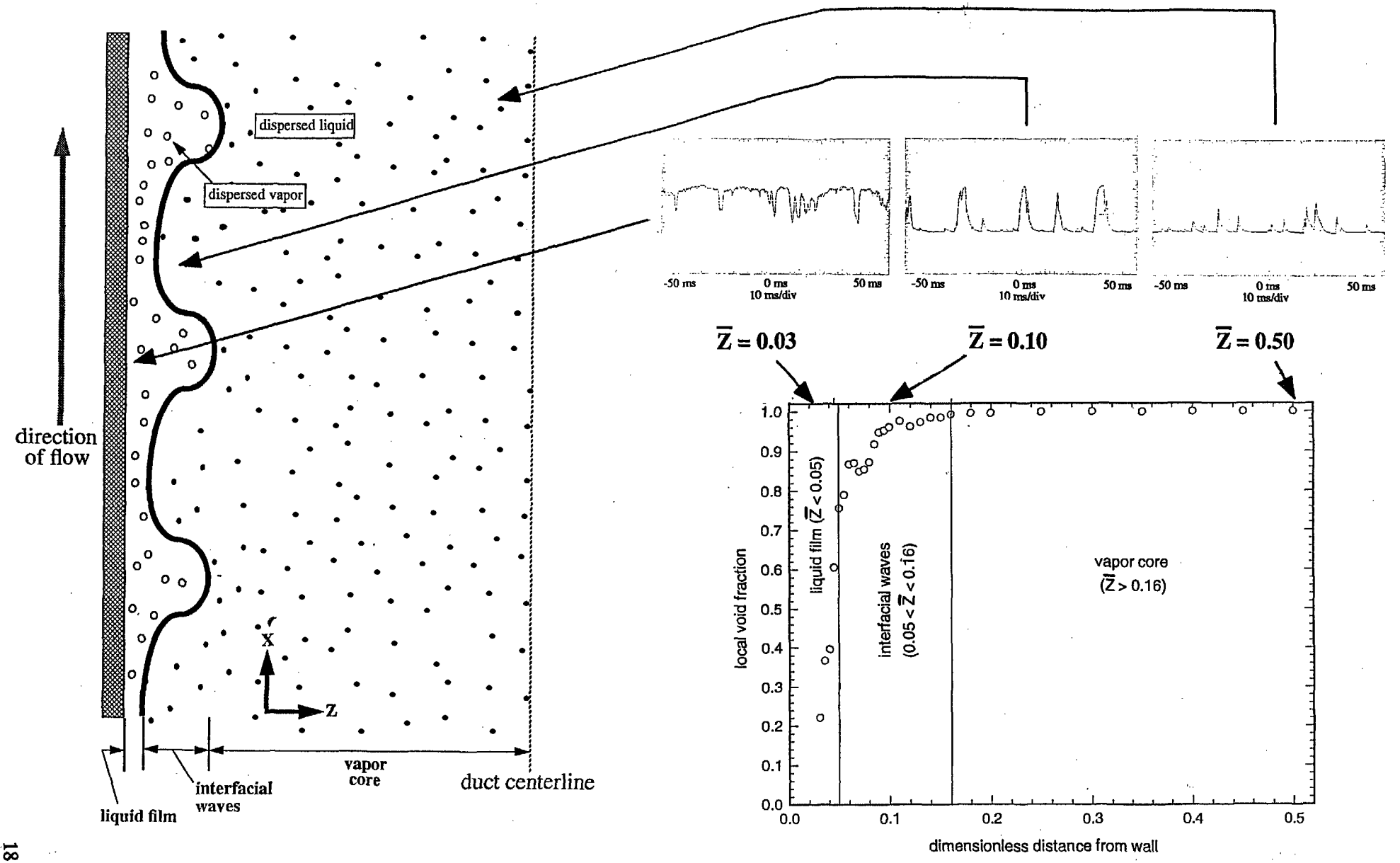

Figure 8 - Regions of Annular Flow Field (Run 61)

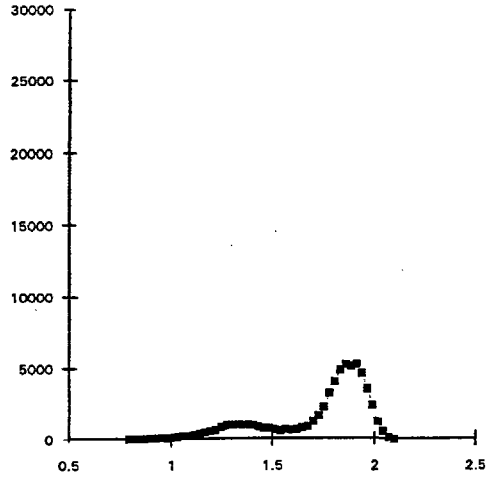

(a) $\overline{Z} = 0.03$

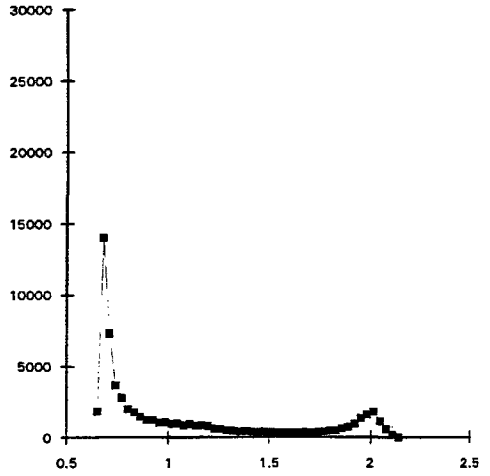

(b) $\overline{Z} = 0.10$

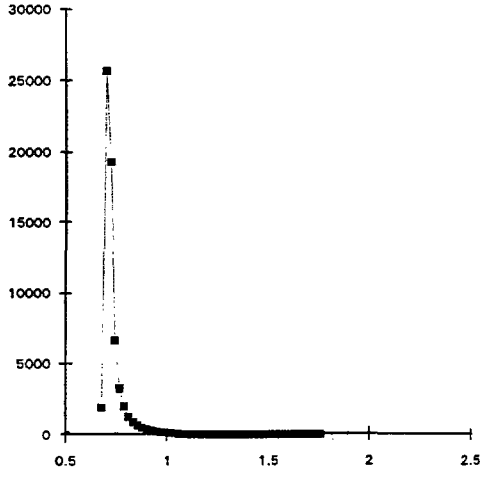

(c) $\overline{Z} = 0.50$

Figure 9 - Voltage Histograms in Annular Flow (Run 61)
abscissa = voltage; ordinate = number of samples

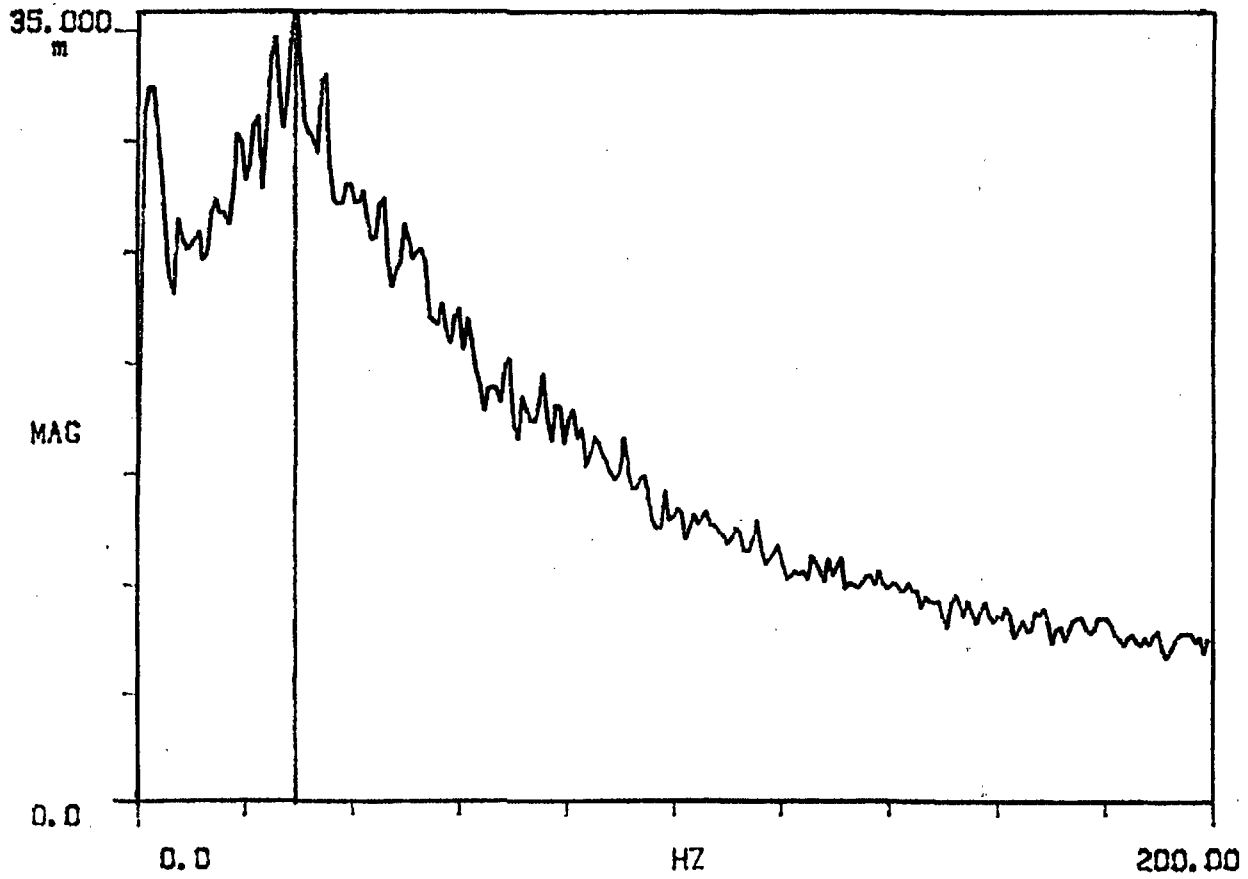

Figure 10 - Autocorrelation in Interfacial Wave Field (Run 69, $\overline{Z} = 0.07$)

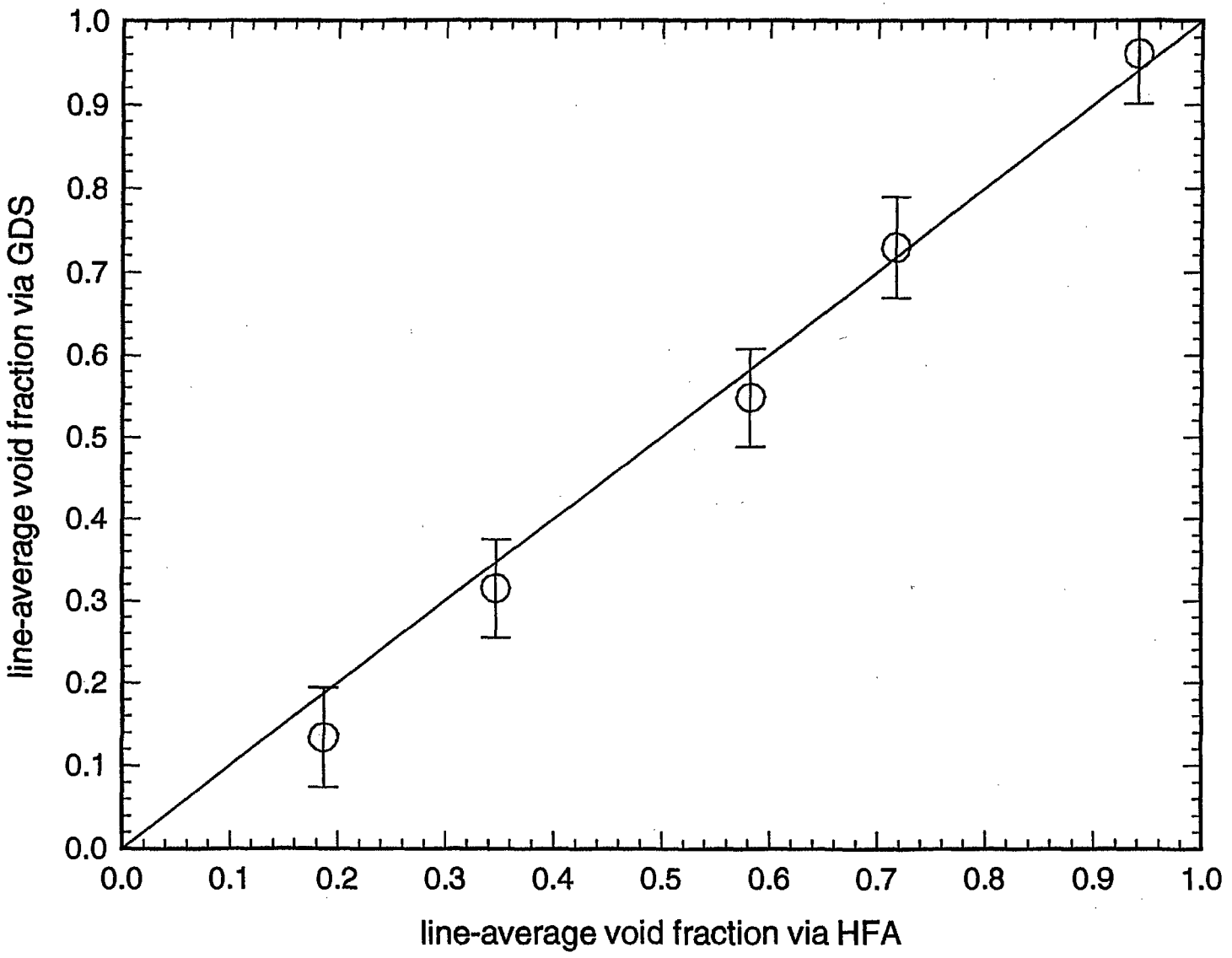

Figure 11 - Comparison of HFA and GDS Void Fraction Measurements